Supplementary Information

for

Interfacial Charge Transfer Modulation in Laser-Synthesized Catalysts for Efficient Oxygen Evolution

Dong Hyeon Lee [a,†], Rahul Kerkar [a,†], Deepak Arumugam [b,†], Jayaraman Theerthagiri [a], Shankar Ramasamy [b], Soorathep Kheawhom [c,*], Myong Yong Choi [a,d,*]

[a] Department of Chemistry (BK21 FOUR), Research Institute of Advanced Chemistry, Gyeongsang National University, Jinju 52828, Republic of Korea

[b] Molecular Simulation Laboratory, Department of Physics, Bharathiar University, Coimbatore 641046, Tamil Nadu, India

[c] Department of Chemical Engineering, Faculty of Engineering, Chulalongkorn University, Bangkok, 10330 Thailand

[d] Core-Facility Center for Photochemistry & Nanomaterials, Gyeongsang National University, Jinju 52828, Republic of Korea

*Correspondence Email address: soorathep.K@chula.ac.th (S. Kheawhom); mychoi@gnu.ac.kr (M.Y. Choi)

[†] These authors contributed equally to this work

Experimental Methods

Materials

All chemicals and reagents utilized in the experiments were employed without further purification. These included iron(III) nitrate nonahydrate ($Fe(NO_3)_3 \cdot 9H_2O$, ≥ 98%, Sigma Aldrich), nickel form (~99.9%, Daejung Chemicals), ethanol (C_2H_5OH, HPLC grade ≥ 99.9%, Daejung Chemicals), potassium hydroxide (KOH, ≥ 93%, Daejung Chemicals), ammonium carbonate ($(NH_4)_2CO_3$, Duksan Pharmaceutical Co. Ltd), and hydrochloric acid (HCl, 35%, Matsunoen Chemicals Ltd).

Characterization techniques

Phase formation and material purity were investigated using X-ray powder diffraction on a Bruker, D8 Advance A25 diffractometer with Cu Kα radiation ($\lambda = 1.54$). The Raman spectroscopic data were recorded on a Thermo Scientific DXR2xi Raman imaging microscope. Morphological studies were conducted using field-emission scanning electron microscopy (FESEM, TESCAN CLARA Field-Emission Scanning Electron Microscope) coupled with energy-dispersive X-ray spectroscopy (EDS) on an Ultim Max system from Oxford Instruments for elemental analysis.

OER study

A membrane-free three-electrode electrochemical setup (CHI 708E electrochemical unit) was employed to study the OER in 1.0 M KOH solution, with an NF-based electrocatalyst as the working electrode, Hg/HgO as the reference, and a graphite rod as the counter electrode. The reference electrode correction was performed using the equation $E_{RHE} = E_{Hg/HgO} + (0.098 + 0.0591 \times pH)$. Linear sweep voltammetry (LSV) plots for OER were recorded at 5 mV/s from

1.2–1.9 V vs. reversible hydrogen electrode (RHE). Furthermore, the Tafel slope, obtained from the experimental data, was calculated using the equation $\eta = b \times \log(j/j_0)$, describing the relation between the overpotential (η) and the logarithm of current density (j) normalized to exchange current density (j_0). Electrochemical impedance spectroscopy (EIS) was conducted in the range of 10^{-1}–10^5 Hz at 1.62 V vs. RHE. To evaluate the electrocatalytic performance, the double-layer capacitance (C_{dl}) of the electrodes was first determined, which is proportional to the electrochemically active surface area (ECSA). Then, the available surface active (SA) sites were calculated by integrating the charge under the reduction peak in the cyclic voltammetry (CV) curve and normalizing it by the scan rate and the charge of a single electron. SA was obtained by substituted in the following equation:

$$SA = \frac{((\frac{area\ under\ curve}{2})/scan\ rate)}{charge\ of\ an\ electron}$$

SA was then used to calculate the turnover frequency (TOF), a crucial metric for the intrinsic activity of a catalyst.

TOF values were determined using the following formula:

$$\text{TOF} = (j \times \text{NA}) / (n \times F \times \text{SA}),$$

where j represents the current density, NA is Avogadro's number (6.022×10^{23}), F is the Faraday constant (96485.3 C/mol), and n denotes the number of electrons transferred during the reaction (4 e^-).

Computational details

To investigate the influence of Fe in NiFe LDH, first-principle calculations were performed using density functional theory (DFT) via the Vienna Ab initio Simulation Package (VASP)[1]. The Projector Augmented Wave pseudopotential was used to model the electron–ion

interaction, with the spin-polarized generalized gradient approximation Perdew–Burke–Ernzerhof functional applied for exchange-correlation[2,3]. A Hubbard-U correction (DFT+U method) was incorporated to improve the electronic description of LDHs, adopting U = 3 for both Ni and Fe, as established in the literature[4–7]. To include the long-range van der Waals interaction, Grimme's DFT-D3 correction was employed with Becke–Johnson damping[8]. All calculations utilized a 5 × 5 × 1 Monkhorst–pack k-point scheme, with self-consistence criteria for energy and forces set at 1.0×10^{-5} eV and 0.01 eV/Å, respectively. A 3 × 3 × 1 monolayer of $Ni(OH)_2$ LDH was constructed with a vacuum spacing of 25 Å and the cutoff energy for the plane waves is set to 500 eV. NiFe LDH was constructed by substituting Ni with Fe at a concentration of approximately $Ni_{0.8}$ and $Fe_{0.2}$ in the 3 × 3 × 1 monolayer. The *OH, *O, and *OOH intermediates were adsorbed near the substituted region, and Gibbs free energy for the reactions was calculated as[9–13]

$$\Delta G = \Delta E + \Delta ZPE - T\Delta S - eU + k_B T \ln(pH),$$

where ΔE is the adsorption energy of the intermediates, ΔZPE and ΔS is the change in zero-point energy and entropy, respectively, T is the temperature, e is the charge transfer, U is the applied potential, and $k_B T \ln(pH)$ is the correction term for H ions. All free energy calculations were calculated under standard conditions (U = 0, T = 298.15 K, and pH = 0) using the computational hydrogen electrode model proposed by Nørskov et al.[14,15]. The theoretical η for the OER process is obtained using

$$G_{OER} = max\{\Delta G_1, \Delta G_2, \Delta G_3, \Delta G_4\}$$

and

$$\eta = {}^{G_{OER}}\!/_{e} - 1.23\ V,$$

where ΔG_1,ΔG_2,ΔG_3, and ΔG_4 are the free energy changes during the OER process. Detailed calculations are provided in the supplementary information.

OER calculations

The cohesive energy (E_C) for LDHs are calculated using the relation,

$$E_C = \frac{E_{system} - (m\mu_{Ni} + n\mu_O + o\mu_H + p\mu_{Fe})}{m + n + o + p}$$

Where, E_{system} is the energy of the system, μ_{Ni},μ_O,μ_H and μ_{Fe} are the chemical potential of Ni, O, H and Fe atoms respectively. m,n,o and p are the number of Ni, O, H and Fe atoms present in the system respectively.

Under standard conditions, the computation hydrogen electrode (CHE) model express that

$$H^+ + e^- \rightarrow \frac{1}{2} H_2\,(g)$$

For OER process, the reaction pathway occurs majorly via 4 e^- pathway.

$$H_2O(l) + * \rightarrow OH^* + H^+ + e^-$$

$$OH^* \rightarrow O^* + H^+ + e^-$$

$$O^* + H_2O(l) \rightarrow OOH^* + H^+ + e^-$$

$$OOH^* \rightarrow * + O_2 + H^+ + e^-$$

The change in free energy for the four e^- pathway can be obtained as

$$\Delta G_1 = \Delta G_{OH^*}$$

$$\Delta G_2 = \Delta G_{O^*} - \Delta G_{OH^*}$$

$$\Delta G_3 = \Delta G_{OOH^*} - \Delta G_{O^*}$$

$$\Delta G_4 = 4.92 - \Delta G_{OOH^*}$$

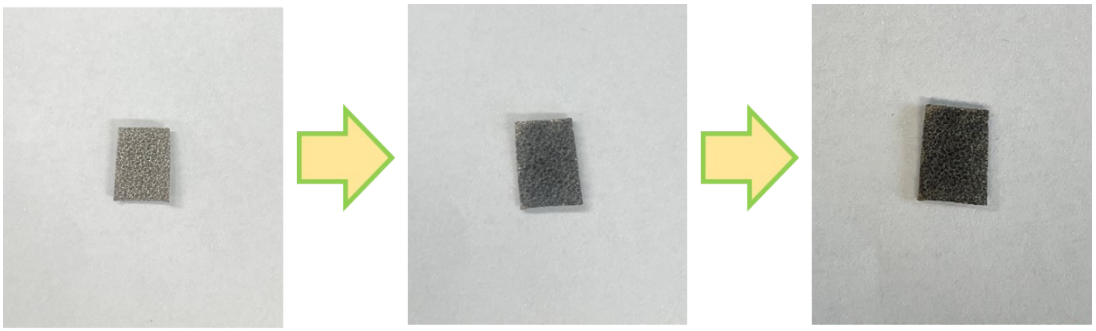

Figure S1. Pictorial representation of bare NF, $Ni(OH)_2$/NF after PLIL, and NiFe LDH/$Ni(OH)_2$/NF after microwave treatment.

Table S1. Change in oxygen concentration in the bare NF, prepared $Ni(OH)_2$/NF, and NiFe LDH/$Ni(OH)_2$/NF fabricated via PLIL and microwave processes.

Sample	O wt%
Bare NF	0.37
$Ni(OH)_2$/NF	3.16
NiFe LDH/$Ni(OH)_2$/NF	21.22

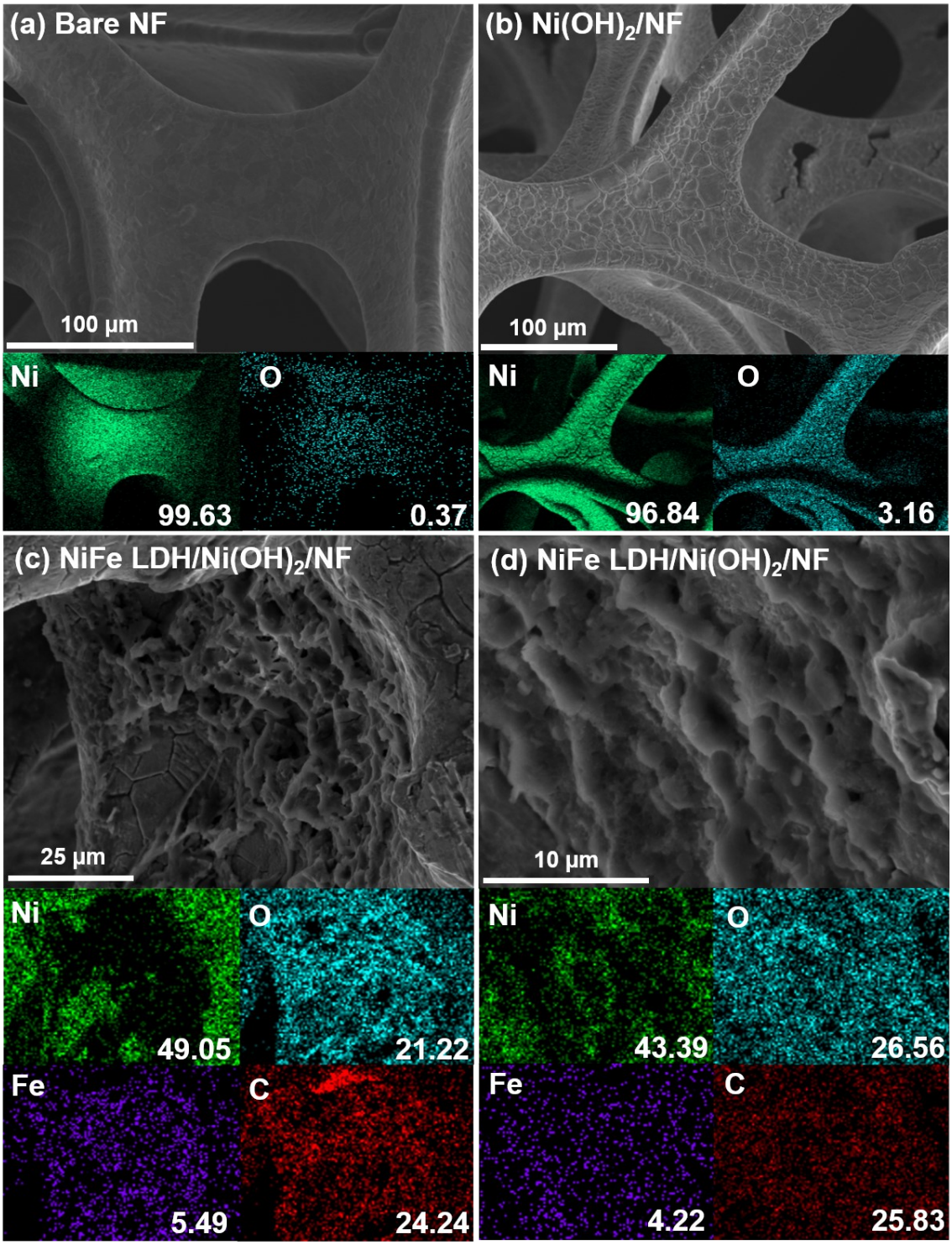

Figure S2. FE-SEM with EDS mapping of the bare NF, $Ni(OH)_2$/NF, and NiFe LDH/$Ni(OH)_2$/NF samples at different magnification.

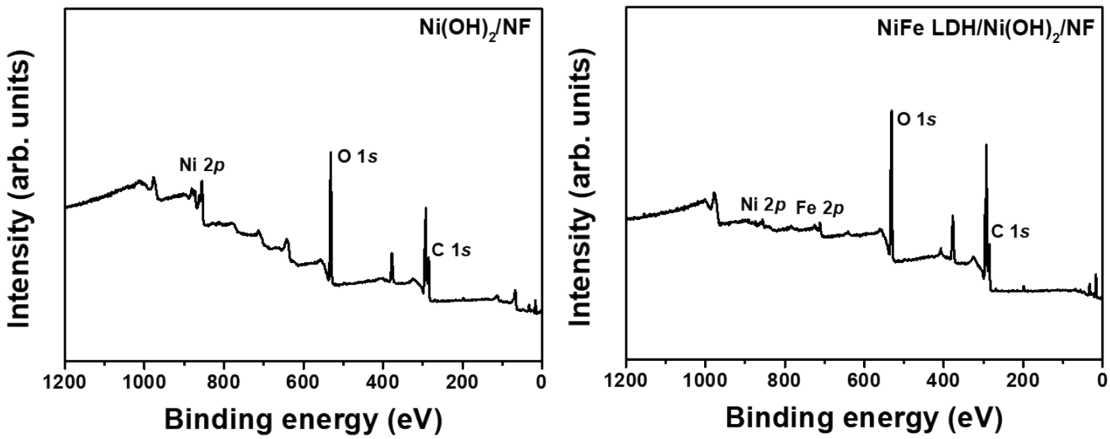

Figure S3. XPS survey spectrum of $Ni(OH)_2$/NF and NiFe LDH/$Ni(OH)_2$/NF samples fabricated via PLIL and microwave processes.

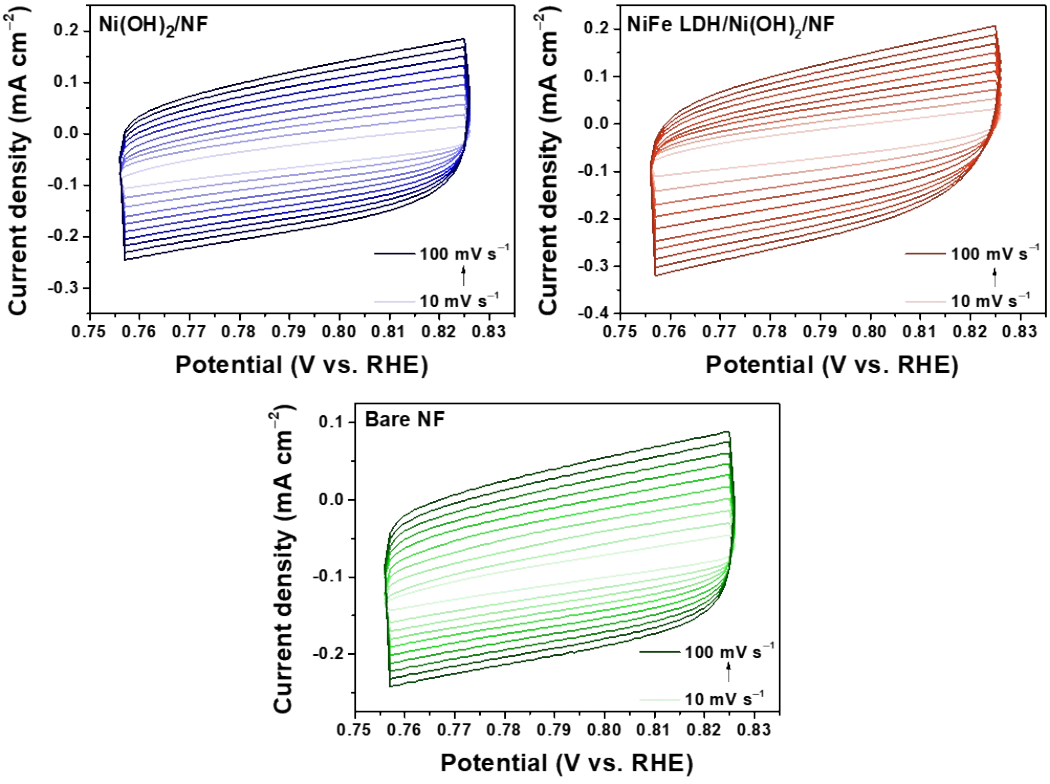

Figure S4. The CV curves measured at different scan rates for NF, $Ni(OH)_2$/NF, and NiFe LDH/$Ni(OH)_2$/NF samples in 1.0 M KOH.

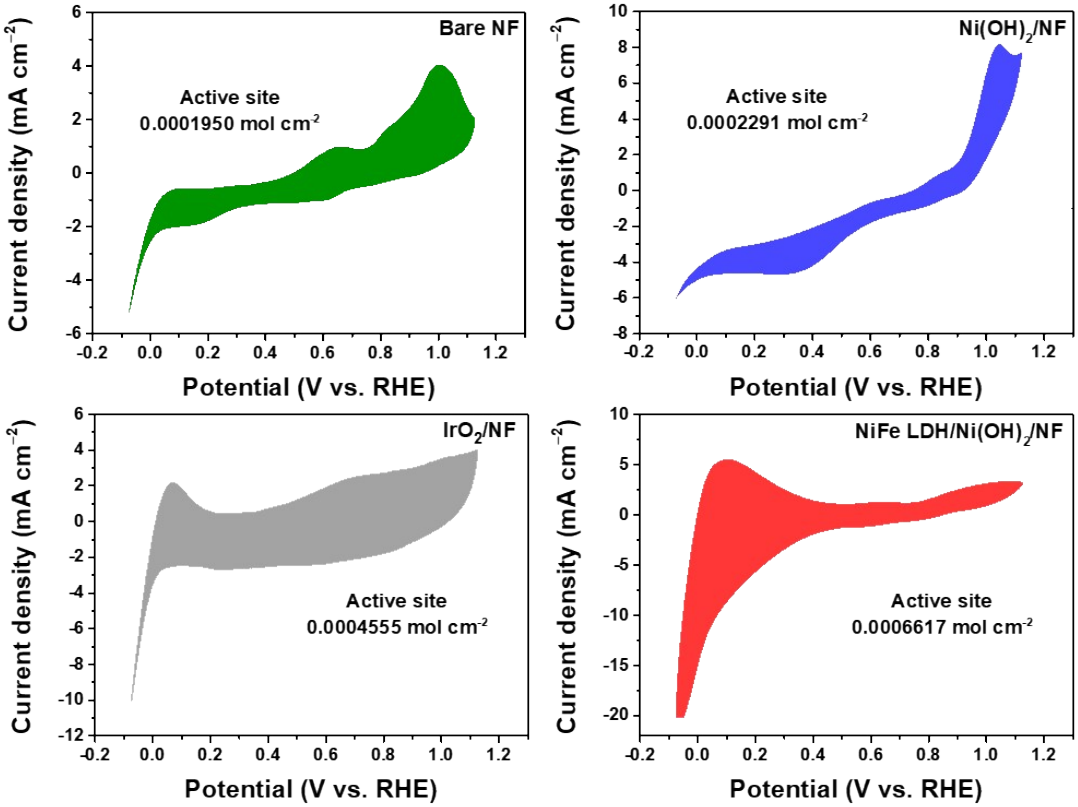

Figure S5. CV curve of NF, $Ni(OH)_2$/NF, and NiFe LDH/$Ni(OH)_2$/NF and the calculated active site values.

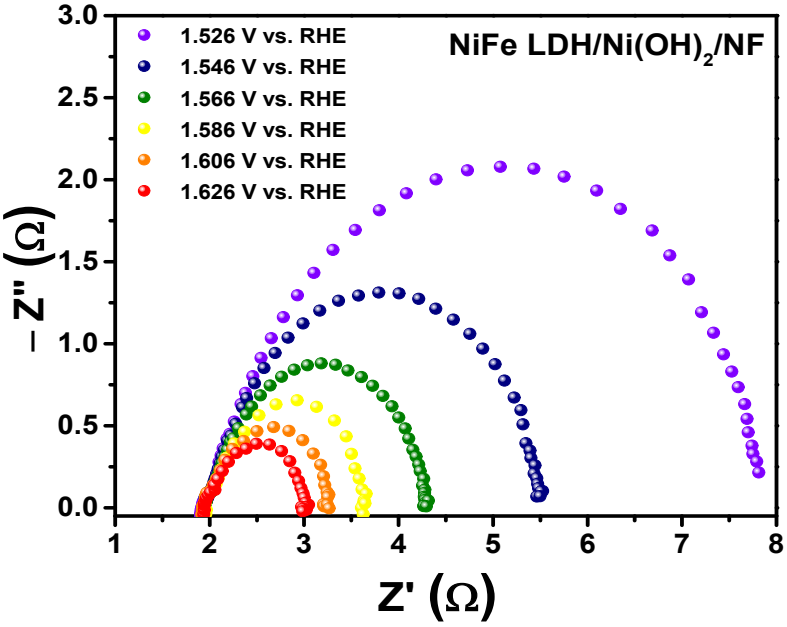

Figure S6. EIS curves for the NiFe LDH/$Ni(OH)_2$/NF at variable potential vs. RHE.

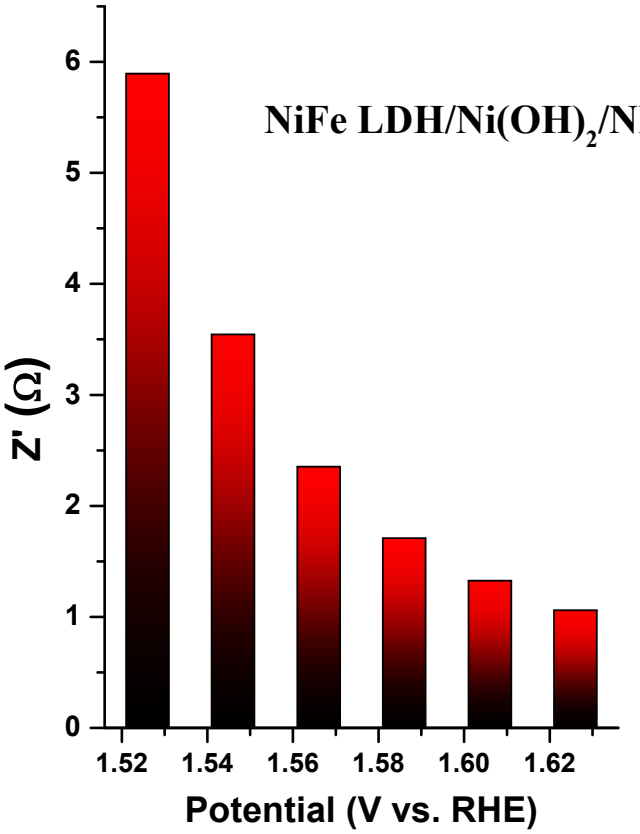

Figure S7. Charge transfer resistance (R_{ct}) values for NiFe LDH/$Ni(OH)_2$/NF at various potentials.

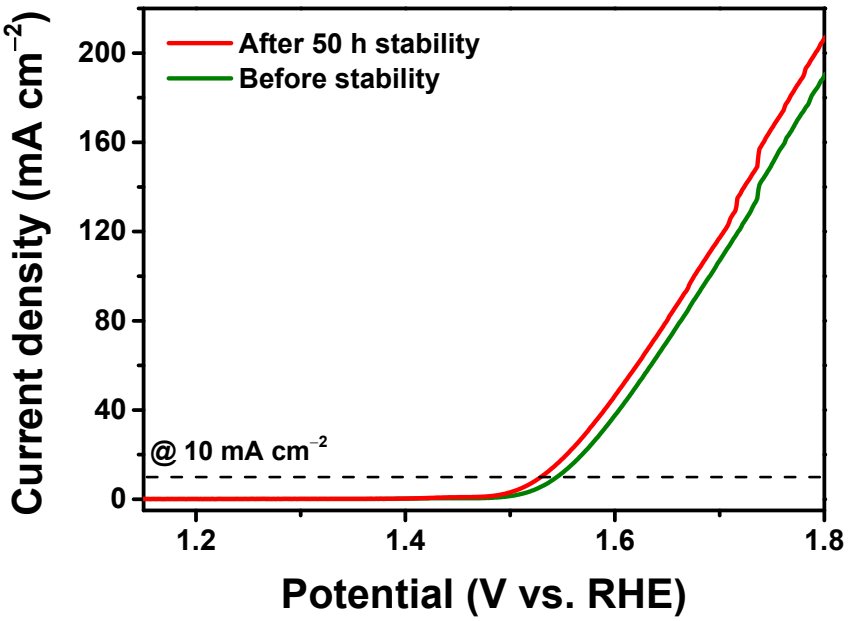

Figure S8. LSV curve of NiFe LDH/$Ni(OH)_2$/NF sample before and after OER stability test.

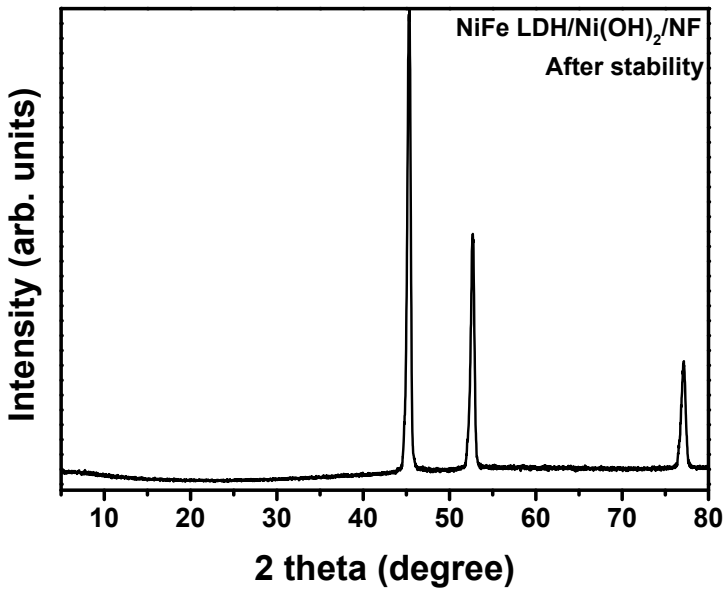

Figure S9. XRD studies of NiFe LDH/$Ni(OH)_2$/NF sample after OER stability test.

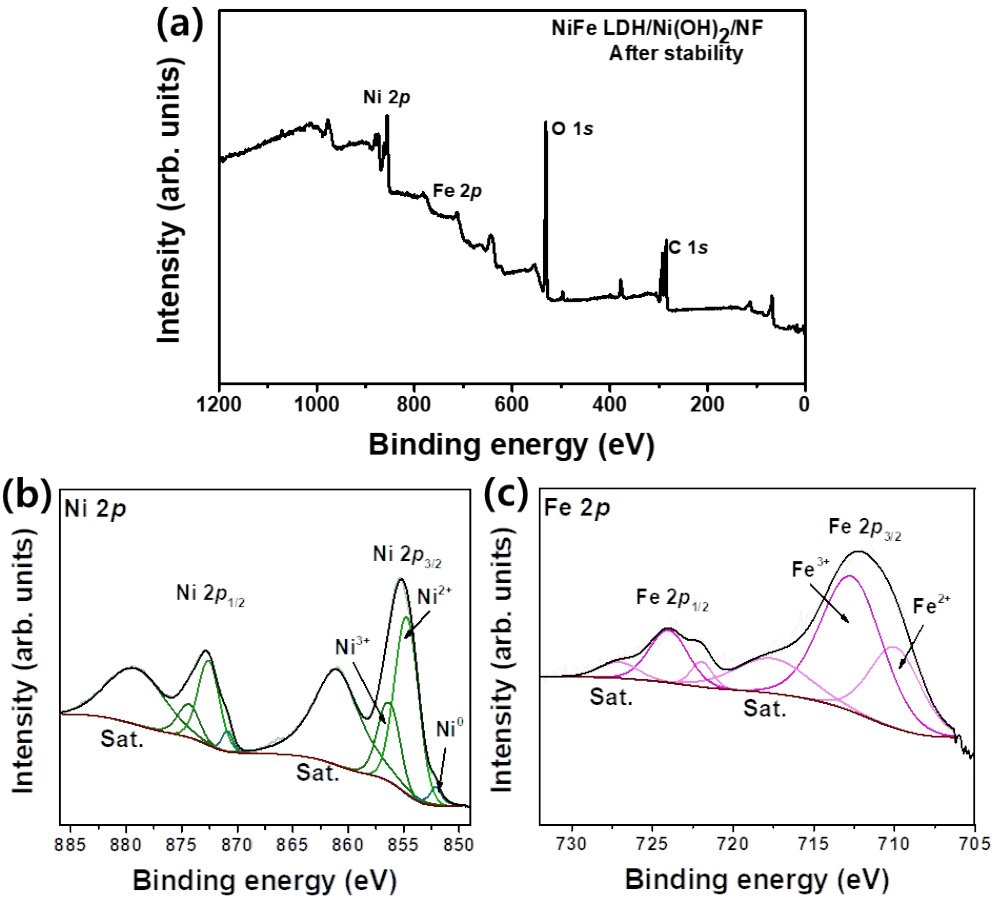

Figure S10. XPS spectra of NiFe LDH/$Ni(OH)_2$/NF sample after OER stability test: (a) Survey scan, (b) Ni 2*p*, and (c) Fe 2*p* core level spectra.

Table S2. Comparison of the OER activity of NiFe LDH/$Ni(OH)_2$/NF and similar composites

Catalyst Name	Synthesis Route	OER Activity (overpotential mV)	References
NiFe LDH@NCP/NF	Electrodeposition Method	281 mV @ 100 mA cm^{-2}	[16]
NiFe-LDH@Co_9S_8-Ni_3S_2/NF	Electroplating Route	223 mV @ 100 mA cm^{-2}	[17]
A/C-NiFe LDH@NFF	Hydrothermal and Electrodeposition Method	359.8 mV @ 1000 mA cm^{-2}	[18]
NiFe-LDH@FeOOH	Chemical Method	259 mV @ 300 mA cm^{-2}	[19]
NiFe-LDH/NF	Electrodeposition Method	223 mV @ 100 mA cm^{-2}	[20]
NiCo-LDH@NiCoS@NiFe-LDH	Electrodeposition Method	209 mV @ 50 mA cm^{-2}	[21]
Co_3O_4 @NiFe-LDH/NF-100	Electrodeposition Method	270 mV @ 50 mA cm^{-2}	[22]
NiFe LDH	Hydrothermal Method	310 mV @ 50 mA cm^{-2}	[23]
NiFe-LDH/SnS	Hydrothermal method	310 mV @ 10 mA cm^{-2}	[24]
NiV-LDH@FeOOH	Hydrothermal method	297 mV @ 100 mA cm^{-2}	[25]
NiFe-LDH/Fe,N-CB	Chemical Method	281 @ 10 mA cm^{-2}	[26]
NiFe LDH-A50	Chemical Method	308 @ 10 mA cm^{-2}	[27]
NiFe LDH/$Ni(OH)_2$/NF	PLIL and Microwave	292 mV @ 10 mA cm^{-2}	Current work

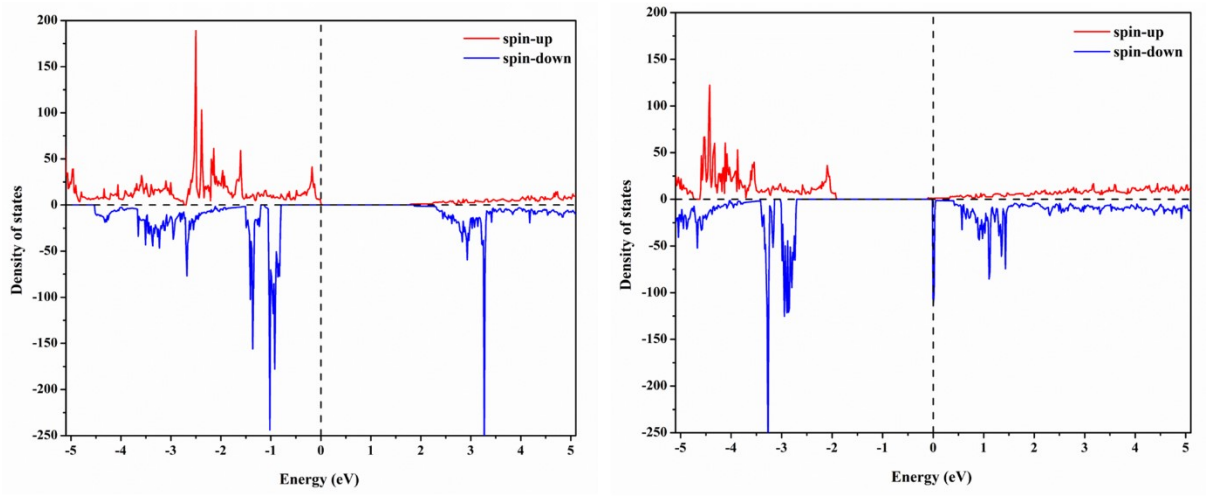

a) b)

Figure S11. Density of states plots of a) $Ni(OH)_2$ and b) $NiFe(OH)_2$

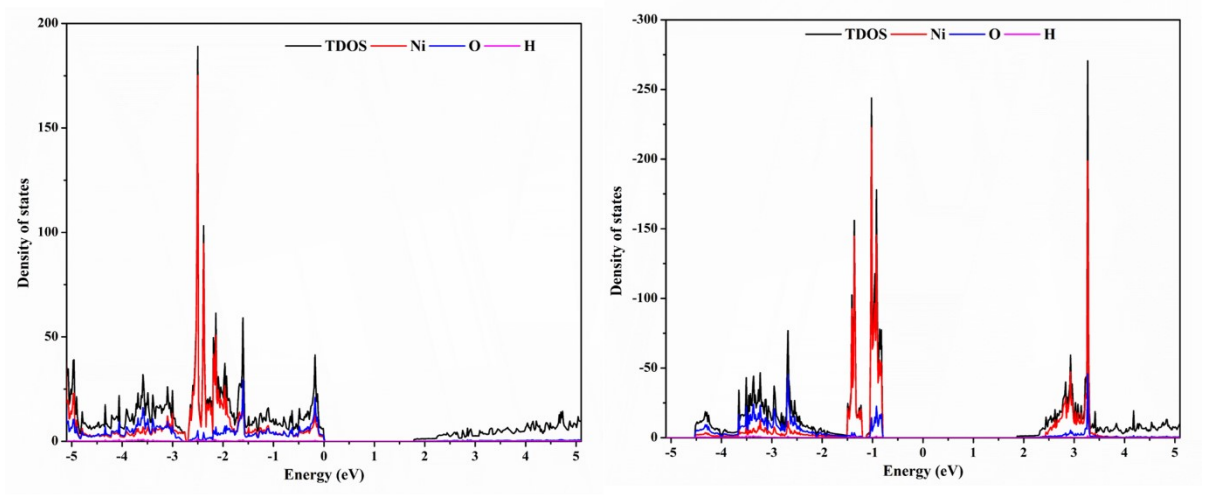

a) b)

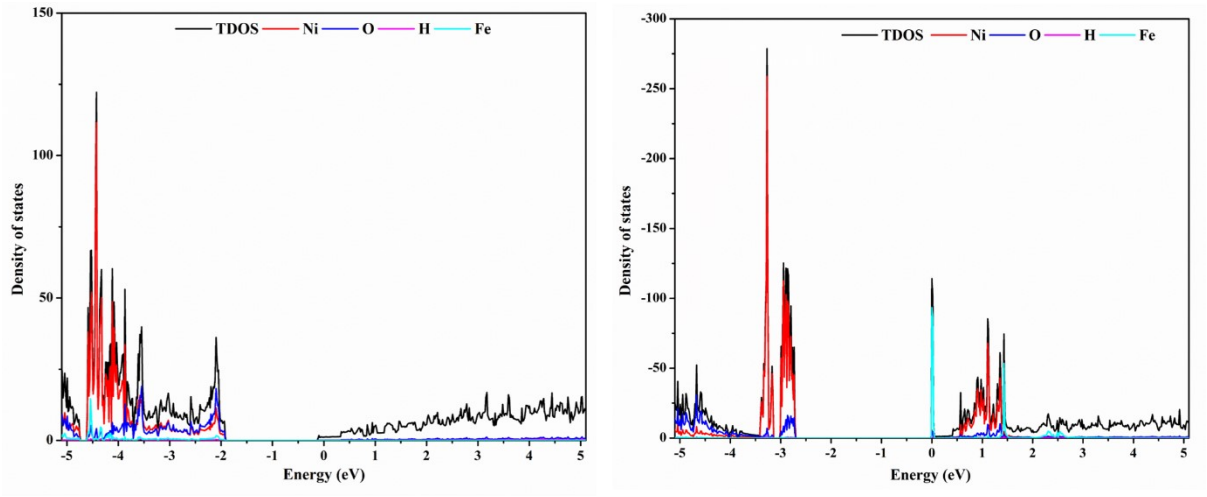

Figure S12. Projected density of states plots of (a) $Ni(OH)_2$ – up, (b) $Ni(OH)_2$ – down, (c) $NiFe(OH)_2$ – up, and (d) $NiFe(OH)_2$ – down.

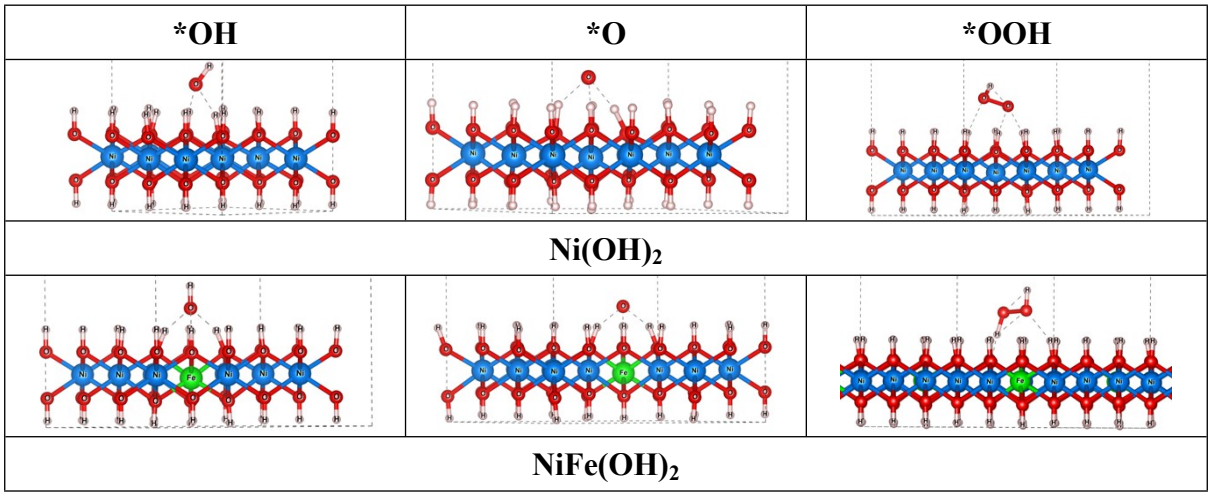

Figure S13. Optimized structures of intermediates adsorbed LDH structures

Table S3. Gibbs free energy change (ΔG) for the intermediates (*OH, *O and *OOH) adsorption

System	Intermediate adsorption (eV)		
	***OH**	***O**	***OOH**
$Ni(OH)_2$	1.45	3.17	4.65
$NiFe(OH)_2$	1.44	2.46	3.57

Table S4. Gibbs free energy change (ΔG) for the OER process and overpotential

System	OER Pathway (eV)				η_{OER} (V)
	ΔG_1	ΔG_2	ΔG_3	ΔG_4	
$Ni(OH)_2$	1.45	1.72	1.48	0.27	0.49
$NiFe(OH)_2$	1.44	1.02	1.11	1.35	0.21

References:

1 G. Kresse and J. Furthmüller, *Phys. Rev. B*, 1996, **54**, 11169–11186.

2 G. Kresse and D. Joubert, *Phys. Rev. B*, 1999, **59**, 1758–1775.

3 J. P. Perdew, K. Burke and M. Ernzerhof, *Phys. Rev. Lett.*, 1996, **77**, 3865–3868.

4 L. Trotochaud, S. L. Young, J. K. Ranney and S. W. Boettcher, *J. Am. Chem. Soc.*, 2014, **136**, 6744–6753.

5 Y. Dong, P. Zhang, Y. Kou, Z. Yang, Y. Li and X. Sun, *Catal. Letters*, 2015, **145**, 1541–1548.

6 V. I. Anisimov, J. Zaanen and O. K. Andersen, *Phys. Rev. B*, 1991, **44**, 943–954.

7 S. L. Dudarev, G. A. Botton, S. Y. Savrasov, C. J. Humphreys and A. P. Sutton, *Phys. Rev. B*, 1998, **57**, 1505–1509.

8 S. Grimme, S. Ehrlich and L. Goerigk, *J. Comput. Chem.*, 2011, **32**, 1456–1465.

9 Y. Wu, C. Li, W. Liu, H. Li, Y. Gong, L. Niu, X. Liu, C. Sun and S. Xu, *Nanoscale*, 2019, **11**, 5064–5071.

10 T. Zhang, B. Zhang, Q. Peng, J. Zhou and Z. Sun, *J. Mater. Chem. A*, 2021, **9**, 433–441.

11 D. Arumugam, J. P. Sivakumar, A. Muralidharan and S. Ramasamy, *Chem. Phys. Impact*, 2024, **9**, 100664.

12 D. Arumugam, M. Subramani, D. Subramani and S. Ramasamy, *Int. J. Hydrogen Energy*, 2024, **68**, 545–558.

13 M. Subramani, A. Rajamani, V. Subramaniam, M. R. Hatshan, S. Gopi and S. Ramasamy, *Environ. Res.*, 2022, **204**, 112114.

14 J. K. Nørskov, T. Bligaard, A. Logadottir, J. R. Kitchin, J. G. Chen, S. Pandelov and U. Stimming, *J. Electrochem. Soc.*, 2005, **152**, J23.

15 A. J. Medford, A. Vojvodic, J. S. Hummelshøj, J. Voss, F. Abild-Pedersen, F. Studt, T. Bligaard, A. Nilsson and J. K. Nørskov, *J. Catal.*, 2015, **328**, 36–42.

16 X. Chen, X. Yu, C. Yang and G. Wang, *J. Solid State Chem.*, 2024, **333**, 124649.

17 L. Liu, Y. Chen, Q. Zhang, Z. Liu, K. Yue, Y. Cheng, D. Li, Z. Zhu, J. Li and Y. Wang, *Appl. Catal. B Environ.*, 2024, **354**, 124140.

18 Y. Li, M. Li, C. Xie, Z. Ling, Y. Lv and K. Chen, *J. Alloys Compd.*, 2024, **1002**, 175328.

19 M. Zhang, B. Wang, H. Sun, M. Chen, T. Zhou, D. Li, B. Xiao, J. Zhao, Y. Zhang, J. Zhang and Q. Liu, *Int. J. Hydrogen Energy*, 2024, **60**, 1215–1223.

20 Y. Wei, Z. Han, T. Liu, X. Ding and Y. Gao, *ChemCatChem*, 2024, **202400447**, 1–6.

21 H. Jiang, H. Qin, P. Zhou, L. Kong, C. Wang, Z. Ji, X. Shen, G. Zhu and A. Yuan, *Int. J. Hydrogen Energy*, 2024, **58**, 892–901.

22 Z. Liu, H. Yuan, Z. Wan, Z. Ma, X. Deng and X. Wang, *J. Alloys Compd.*, 2024, **983**, 173837.

23 Y. Gu, D. H. Park, M. H. Kim, J. H. Byeon, D. M. Lim, S. H. Park, J. H. Kim, J. S. Jang and K. W. Park, *Chem. Eng. J.*, 2024, **480**, 147789.

24 Y. Sun, Q. Cai, Z. Wang, Z. Li, Q. Zhou, X. Li, D. Zhao, J. Lu, S. Tian, Y. Li and S. Wang, *ACS Appl. Mater. Interfaces.*, 2024, DOI:10.1021/acsami.3c18458.

25 W. Bao, L. Xiao, J. Zhang, Z. Deng, C. Yang, T. Ai and X. Wei, *Chem. Commun.*, 2020, **56**, 9360–9363.

26 Y. Wang, Y. Gao, L. Ma, Y. Xue, Z. H. Liu, H. Cui, N. Zhang and R. Jiang, *ACS Appl. Mater. Interfaces*, 2023, **15**, 16732–16743.

27 C. Peng, N. Ran, G. Wan, W. Zhao, Z. Kuang, Z. Lu, C. Sun, J. Liu, L. Wang and H. Chen, *ChemSusChem*, 2020, **13**, 811–818.